Mechanistic model of cardiac energy metabolism predicts localization of glycolysis to cytosolic subdomain during ischemia

Lufang Zhou, Jennifer E. Salem, Gerald M. Saidel, William C. Stanley and Marco E. Cabrera

AJP - Heart 288:2400-2411, 2005. First published Jan 28, 2005; doi:10.1152/ajpheart.01030.2004

AJP - Heart and Circulatory Physiology publishes original investigations on the physiology of the heart, blood vessels, and lymphatics, including experimental and theoretical studies of cardiovascular function at all levels of organization ranging from the intact animal to the cellular, subcellular, and molecular levels. It is published 12 times a year (monthly) by the American Physiological Society, 9650 Rockville Pike, Bethesda MD 20814-3991. Copyright © 2005 by the American Physiological Society. ISSN: 0363-6135, ESSN: 1522-1539. Visit our website at http://www.the-aps.org/.

Am J Physiol Heart Circ Physiol 288: H2400–H2411, 2005.
First published January 28, 2005; doi:10.1152/ajpheart.01030.2004.

Mechanistic model of cardiac energy metabolism predicts localization of glycolysis to cytosolic subdomain during ischemia

Lufang Zhou,[1,4] Jennifer E. Salem,[3,4] Gerald M. Saidel,[1,4] William C. Stanley,[2,4] and Marco E. Cabrera[1,2,3,4]

Departments of [1]Biomedical Engineering, [2]Physiology and Biophysics, and [3]Pediatrics and [4]Center for Modeling Integrated Metabolic Systems, Case Western Reserve University, Cleveland, Ohio

Submitted 7 October 2004; accepted in final form 27 December 2004

Zhou, Lufang, Jennifer E. Salem, Gerald M. Saidel, William C. Stanley, and Marco E. Cabrera. Mechanistic model of cardiac energy metabolism predicts localization of glycolysis to cytosolic subdomain during ischemia. *Am J Physiol Heart Circ Physiol* 288: H2400–H2411, 2005. First published January 28, 2005; doi:10.1152/ajpheart.01030.2004.—A new multidomain mathematical model of cardiac cellular metabolism was developed to simulate metabolic responses to reduced myocardial blood flow. The model is based on mass balances and reaction kinetics that describe transport and metabolic processes of 31 key chemical species in cardiac tissue. The model has three distinct domains (blood, cytosol, and mitochondria) with interdomain transport of chemical species. In addition to distinguishing between cytosol and mitochondria, the model includes a subdomain in the cytosol to account for glycolytic metabolic channeling. Myocardial ischemia was induced by a 60% reduction in coronary blood flow, and model simulations were compared with experimental data from anesthetized pigs. Simulations with a previous model without compartmentation showed a slow activation of glycogen breakdown and delayed lactate production compared with experimental results. The addition of a subdomain for glycolysis resulted in simulations showing faster rates of glycogen breakdown and lactate production that closely matched in vivo experimental data. The dynamics of redox ($NADH/NAD^+$) and phosphorylation (ADP/ATP) states were also simulated. These controllers are coupled to energy transfer reactions and play key regulatory roles in the cytosol and mitochondria. Simulations showed a similar dynamic response of the mitochondrial redox state and the rate of pyruvate oxidation during ischemia. In contrast, the cytosolic redox state displayed a time response similar to that of lactate production. In conclusion, this novel mechanistic model effectively predicted the rapid activation of glycogen breakdown and lactate production at the onset of ischemia and supports the concept of localization of glycolysis to a subdomain of the cytosol.

redox state; computer simulation; cytosol; mitochondria; metabolic channeling

THE PRIMARY EFFECT of myocardial ischemia is impaired oxidative phosphorylation due to decreased oxygen delivery to the mitochondria (68). Reduced aerobic ATP production stimulates glycogen breakdown and ATP formation from glycolysis in the cytosol and results in lactate accumulation in the tissue (52, 68). Various metabolites related to energy transfer (e.g., $NADH$-NAD^+ and ADP-ATP) act as modulators of key reactions in the cytosol and mitochondria but have different concentrations in these cellular domains. For example, under aerobic conditions, 5–10% of total ATP (10, 62) and 90% of the NAD^+ and NADH (61) are in the mitochondria. On the basis of this evidence, it is inappropriate to assume the same concentrations of these metabolites in the cytosol and mitochondria when studying mechanisms controlling glycolysis and lactate metabolism from normal to ischemic conditions. Furthermore, it has been observed that key glycolytic enzymes are bound together in specific intracellular structures to form a multienzyme complex near the sarcolemma and sarcoplasmic reticulum (8, 19, 42). Because the glycolytic enzymes are not freely distributed, glycolysis can be considered localized in a subdomain within the cytosol.

Unfortunately, at present, it is not feasible to measure dynamic changes in the fluxes and concentrations of key cytosolic and mitochondrial species in the transition from normal to ischemic conditions with current experimental techniques. As an alternate approach to conducting experimental measurements and as a framework for quantitative analysis of in vivo myocardial cellular metabolism, a physiological-based mathematical model that incorporates mechanistic details can be used to predict nonobservable variables. A previous model (59) of cardiac metabolism predicted many of the key species concentration and flux changes observed during moderate ischemia. Because the model structure consisted of a single cellular compartment, processes in the cytosol could not be distinguished from those in the mitochondria. This model was able to simulate steady-state responses to ischemia that were in agreement with experimental observations from large animal models, such as the changes in oxygen consumption. However, it poorly predicted the dynamics of glycogen breakdown, glycolysis, and the switch from myocardial lactate uptake to release observed at the onset of ischemia in validation studies performed in swine (59).

To simulate these observations and predict other responses, a more general multidomain model was developed that *1*) distinguishes cytosol and mitochondria with species transport across the sarcolemmal and mitochondrial membranes, *2*) includes additional chemical species that participate in the regulation of energy metabolism (e.g., P_i), and *3*) incorporates more detail in metabolic pathways [e.g., glycolysis and the tricarbocylic acid (TCA) cycle]. Furthermore, to simulate the activation of glycolysis in response to ischemia, we postulated a subcellular region within the cytosol that permits metabolic channeling to occur in the glycolytic pathway. By simulating cytosolic and mitochondrial species concentration dynamics, this model provided the basis for quantifying the mechanisms controlling the rate of glycogen breakdown and glycolysis as well as lactate formation and exchange during the transition from normal to ischemic conditions. Therefore, to test the

Address for reprint requests and other correspondence: M. E. Cabrera, Pediatric Cardiology, Rainbow Babies and Children's Hospital, 11100 Euclid Ave., RBC-389, Cleveland, OH 44106-6011 (E-mail: mec6@case.edu).

The costs of publication of this article were defrayed in part by the payment of page charges. The article must therefore be hereby marked "*advertisement*" in accordance with 18 U.S.C. Section 1734 solely to indicate this fact.

existence of an intracellular structure that contains all the key glycolytic enzymes bound together forming a multienzyme complex, we added a subdomain within the cytosol in our current model of myocardial metabolism. In the following sections, the model development is described and computer simulations are compared with data from in vivo experiments performed in a well-characterized swine model (58, 65). The covariations of key cytosolic and mitochondrial concentrations and flux rates are then analyzed to elucidate the mechanisms of regulation and to suggest future critical experiments.

MODEL DEVELOPMENT

Although physiological modeling of the heart began over 40 years ago, this field still lacks a comprehensive model of cardiac energy metabolism. Existing models incorporate some aspects of glycolysis, the TCA cycle, and oxidative phosphorylation, but none of them integrate all these pathways (1, 15, 16). Several comprehensive models of metabolism exist for other systems rather than the heart. Joshi and Palsson (35) developed a model of red blood cell metabolism that included glycolysis, the pentose pathway, and nucleotide metabolism. Cabrera et al. (13, 14) developed a model of muscle metabolism that included glycolysis, glycogenolysis and glycogenesis, and pyruvate oxidation and oxidative phosphorylation using a whole body top-down approach and studied the effects of hypoxic and ischemic conditions. These models all contained some aspects that are necessary to be included in a model of myocardium metabolism, such as reactions considered, control mechanisms, or the modeling technique. However, they are limited to the study of glycolysis and the TCA cycle with carbohydrate as the sole fuel substrate. Salem et al. (59) developed a comprehensive model of cardiac metabolism that included glycolysis and fatty acid oxidation as well as oxidative phosphorylation; however, this model still missed some key regulatory metabolites (e.g., P_i) and lumped the cytosol and mitochondria. Therefore, the goal of this study was to extend a previous developed and validated model of cardiac metabolism (59) and to improve its predicting power by including essential subcellular compartments and appropriate transport processes across their membranes. Our approach was to combine the development of a comprehensive mathematical model of human cardiac metabolism and in vivo experimental measurements in large mammals (e.g., swine) that have been demonstrated to have similar responses as the human heart. Models with similar approaches have been used previously to describe complex metabolic systems with species transport and biochemical reactions (13, 14, 39, 59).

Model domains. To simulate the metabolic processes that occur inside the heart during ischemia, a general mathematical model was developed that represents the heart as perfused tissue with a characteristic cell having distinct cytosolic and mitochondrial domains (Fig. 1). In the perfused tissue, convective mass transport occurs in the blood capillaries, whereas passive transport occurs between blood plasma and interstitial fluid. Typically, the characteristic time for capillary-interstitial transport is much shorter than that for convection through the capillaries (28) so that local chemical equilibrium between plasma and interstitial fluid is approximately valid. Therefore, we considered the perfused tissue to have one extracellular domain consisting of blood plasma and interstitial fluid, which for simplicity is called "blood." Within the extravascular tissue cells, we distinguished two domains: the cytosol and mitochondria. Between domains (blood-cytosol and cytosol-mitochondria), molecular transport can occur by passive diffusion or carrier-mediated transport (9, 32, 38). This multidomain model diagram is shown in Fig. 2. Furthermore, a smaller region of the cytosol is considered as the subdomain of the reactions in the glycolytic pathway, and equilibrium is assumed between the subdomain and cytosol for the related metabolites, e.g., glucose, lactate, and pyruvate. The detailed biochemical reactions in each domain are described in Table 1.

Metabolic system components. Many chemical species are essential for simulating accurately the dynamic metabolic response of myocardium to ischemia. Under normal conditions, the main fuels of the heart are free fatty acids and carbohydrates, primarily glucose and lactate. Other key metabolites include glycogen, glucose-6-phosphate, glyceraldehyde-3-phosphate, 1,3-bisphospho-glycerate, pyruvate, triglyceride, glycerol, fatty acyl-CoA, acetyl-CoA, and free CoA. Species involved in the TCA cycle are citrate, α-ketoglutarate, succinyl-CoA, succinate, malate, and oxaloacetate. The species involved in tissue-gas exchange are O_2 and CO_2, whereas those involved in energy transfer and metabolic regulation are P_i, creatine, phosphocreatine, NAD^+, NAD, ATP, and ADP.

Dynamic mass balances. The concentration dynamics of chemical species in the blood, cytosol, and mitochondria can be described by a mathematical model based on mass balances, passive and carrier-mediated transport processes, and distinctive chemical reactions, especially those involved in energy transfer processes. In the "blood" domain, arterial blood carries fuels and oxygen, whereas venous blood takes away metabolic products (e.g., CO_2) from the heart. The dynamic mass balance equation for *species j* can be written as (14, 59):

$$V_b \frac{dC_{bj}}{dt} = Q(C_{aj} - C_{vj}) - J_{b\rightarrow c,j} \qquad (1)$$

where V_b is the domain volume, Q is blood flow, $C_{aj}(t)$ is the arterial concentration of *species j*, $C_{vj}(t)$ is the venous concentration of *species j*, and $J_{b\rightarrow c,j}$ is the mass transport rate of *species j* from the blood to cytosol. For cardiac metabolism, only some of the species are considered to be exchanged between blood and cytosol (Fig. 1); for those that exist only in the cell, this equation disappears.

The average "blood" concentration $C_{bj}(t)$ can be approximated as a linear combination of the arterial and venous concentrations (47):

$$C_{bj} = FC_{vj} + (1 - F)C_{aj} \rightarrow C_{vj} = \frac{C_{bj} - (1 - F)C_{aj}}{F} \qquad (2)$$

where F is the mixing fraction. For perfect mixing, $F = 1$ and $C_{bj} = C_{vj}$; with no mixing, $F = 0$ and $C_{bj} = C_{aj}$. Substituting *Eq. 2* into *Eq. 1*, we obtain

$$V_b \frac{dC_{bj}}{dt} = \frac{Q(C_{aj} - C_{bj})}{F} - J_{b\rightarrow c,j} \qquad (3)$$

In the cytosolic domain, the concentration of *species j* may change as a result of metabolic reactions and mass transfer

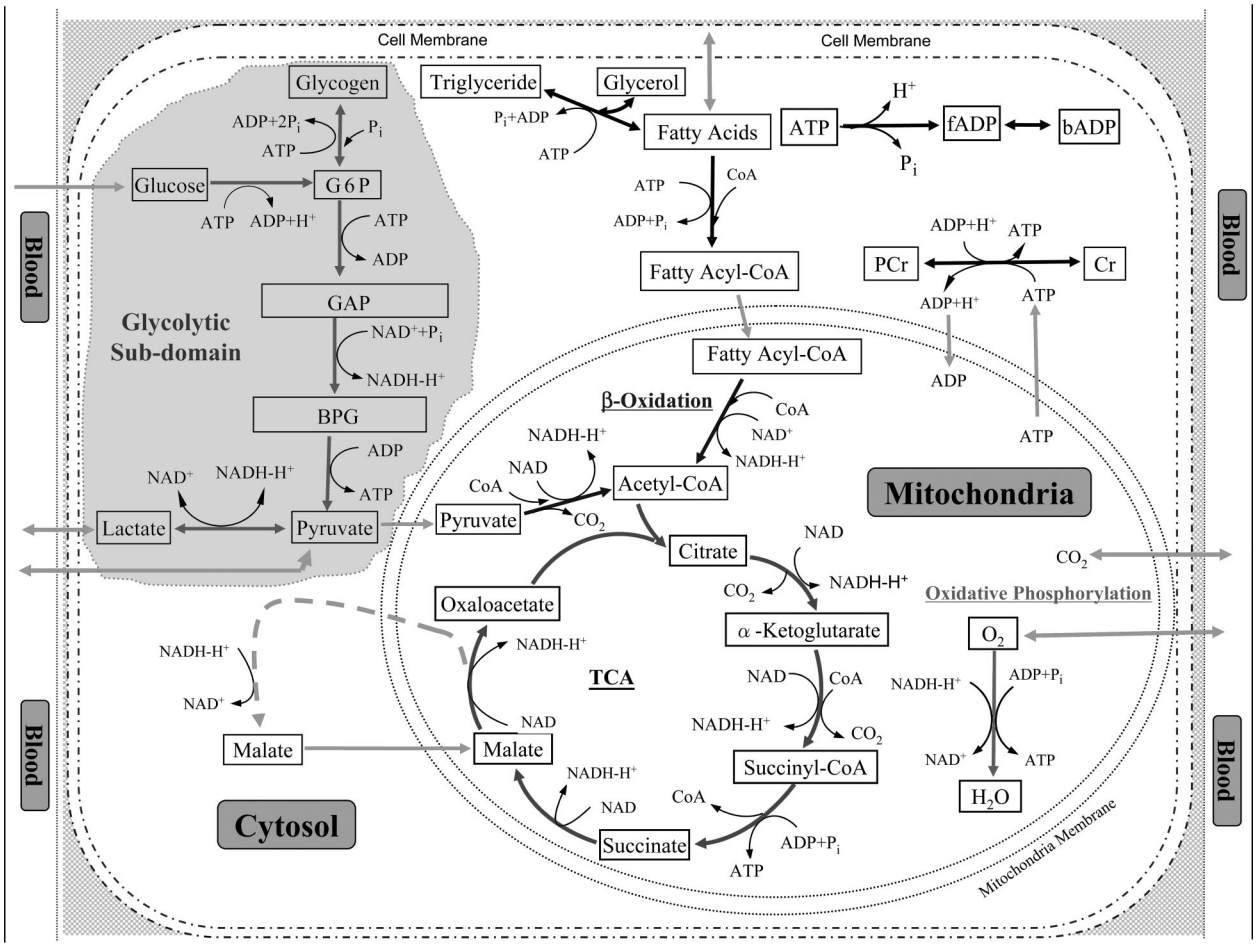

Fig. 1. Detailed biochemical pathway map of cardiac metabolism. It is a complex network of biochemical reactions and pathways including glycolysis, pyruvate oxidation, fatty oxidation, the tricarboxylic acid (TCA) cycle, and oxidative phosphorylation. It also includes species transport across cellular and mitochondrial membranes. G6P, glucose-6-phosphate; GAP, glyceraldehyde-3-phosphate; BPG, 1,3-bisphospho-glycerate; Cr, creatine; PCr, phosphocreatine.

across the cellular membrane and mitochondrial membrane (59):

$$V_{cj}\frac{dC_{cj}}{dt} = R_{cj} + J_{b\to c,j} - J_{c\to m,j} \quad (4)$$

where V_{cj} is the effective volume of *species j* in the cytosol and C_{cj} is the concentration is *species j* in the cytosol. R_{cj} is the metabolic reaction rate of *species j*, and $J_{c\to m,j}$ is the mass transport rate of *species j* from the cytosol to mitochondria. For those species that are not transported across the cellular and/or the mitochondrial membrane, the corresponding transport term(s) vanish.

In the mitochondrial domain, the dynamic mass balance equation for *species j* is (59)

$$V_{mj}\frac{dC_{mj}}{dt} = R_{mj} + J_{c\to m,j} \quad (5)$$

where V_{mj} is the effective volume of *species j* in the mitochondrial domain, C_{mj} is the concentration of *species j* in the mitochondiral domain, and R_{mj} is the net reaction rate of *species j*. For those species that exist in the mitochondria only, the last term in the right side vanishes.

Interdomain transport. Some species are transported between domains "*x*" and "*y*" by passive diffusion, and the transport rate ($J^{p}_{x\to y,j}$), is given by (63a)

$$J^{p}_{x\to y,j} = \lambda_{x\to y,j}(C_{x,j} - \sigma_{x\to y,j}C_{y,j}) \quad (6)$$

where $\lambda_{x\to y,j}$ is the membrane transport coefficient that incorporates membrane permeability and effective surface area and $\sigma_{x\to y,j}$ is the partition coefficient. Passive diffusion through a membrane is a nonsaturable process that is linearly related to substrate concentrations on both sides of the membrane. The transport of other substrates (e.g., glucose), however, displays saturation kinetics associated with a carrier-mediated mechanism (37). The rate of carrier-mediated transport can be expressed using a Michaelis-Menten equation that characterizes enzyme kinetics (32)

$$J^{f}_{x\to y,j} = \frac{T_{x\to y,j}C_{x,j}}{M_{x\to y,j} + C_{x,j}} \quad (7)$$

where $T_{x\to y,j}$ is the transport rate coefficient and $M_{x\to y,j}$ is the affinity coefficient.

Metabolic reaction rates. The net reaction rate of *species j* in *domain x*, R_{xj}, can be represented as the difference of rates of species production P_{xj} and utilization U_{xj} (59):

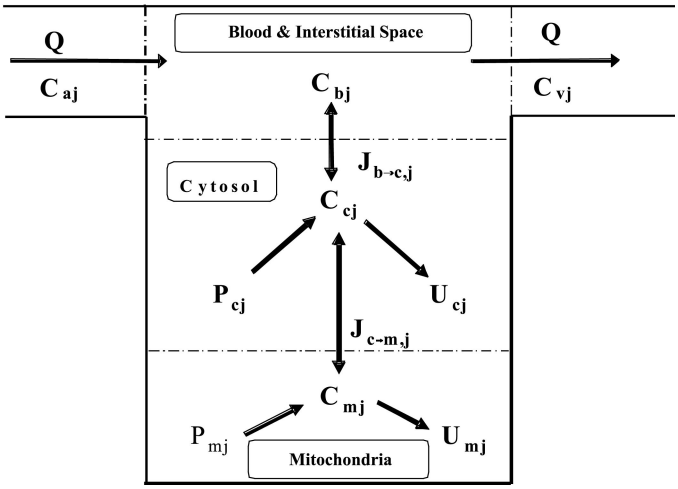

Fig. 2. Blood-cell transport processes and metabolic reactions. Reversible arrow indicates species transport between domains. The transport can be either passive diffusion (viz., fatty acid, O_2, and CO_2) or carrier mediated (viz., glucose, ATP/ADP, P_i, NADH/NAD, lactate, pyruvate oxalocaetate, malate, and fatty acyl CoA). Q, blood flow; C_{aj}, arterial concentration of *species j*; C_{vj}, venous concentration of *species j*; C_{bj}, concentration of *species j* in the blood; $J_{b\rightarrow c,j}$, mass transport rate of *species j* from the blood to cytosol; C_{cj}, concentration of *species j* in the cytosol; P_{cj}, rate of *species j* production in the cytosol; U_{cj}, rate of *species j* utilization in the cytosol; C_{mj}, concentration of *species j* in the mitochondria; P_{mj}, rate of *species j* production in the mitochondria; U_{mj}, rate of *species j* utilization in the mitochondria.

$$R_{xj} = P_{xj} - U_{xj} = \sum_{k=1}^{n} \beta_{k,j}\phi_{k,j} - \sum_{k=1}^{m} \beta_{j,k}\phi_{j,k} \qquad (8)$$

where $\phi_{k,j}$ is the reaction flux from *species k* to *species j*, $\beta_{k,j}$ is the corresponding stoichiometric coefficient, n is the number of reaction fluxes forming *species j* from *species k*, and m is the number of reaction fluxes that consume *species j* to produce *species k*. The net reaction rate for each chemical species in the cytosol and mitochondria are listed in Table 2. As a general reaction, we consider reactants X and Y and products Z and W with the corresponding metabolic controllers E_1 and E_2:

$$X + Y \xrightarrow{E_1 \quad E_2} Z + W$$

The corresponding reaction flux is assumed to have a general Michaelis-Menten form (32)

$$\phi_{X-Y,z-W} = \frac{V_{X-Y,Z-W}C_XC_Y}{K_{X-Y,Z-W} + C_XC_Y}\left(\frac{PS^{\pm}}{\mu^{\pm} + PS^{\pm}}\right)\left(\frac{RS^{\pm}}{\nu^{\pm} + RS^{\pm}}\right) \qquad (9)$$

where $K_{X\rightarrow Y,Z\rightarrow W}$ and $V_{X\rightarrow Y,Z\rightarrow W}$ are Michaelis-Menten coefficients specific to the reaction process. In this model, the two coupled controllers are the phosphorylation state $PS^+ = C_{ATP}/C_{ADP}$ and the redox state $RS^+ = C_{NADH}/C_{NAD}$, where C indicates the concentration. Here, ADP represents free (or active) ADP. In the cytosol, most ADP is bound to macromolecules (e.g., actin monomer) to form the bound ADP, but only free ADP participates in metabolic reactions. For some reac-

Table 1. *Biochemical-reactions*

	Overall Reaction	Substrate Reaction	Coupled Reaction
Reactions in cytosol			
GLU utilization	GLU + ATP → G6P + ADP + H^+	GLU → G6P + H^+	ATP → ADP
GLY synthesis	G6P + ATP → GLY + ADP + $2P_i$	G6P → GLY + P_i	ATP → ADP + P_i
GLY utilization	GLY + P_i → G6P		
G6P breakdown	G6P + ATP → 2GAP + ADP	G6P → 2GAP	ATP → ADP
GAP breakdown	GAP + NAD^+ + P_i → BPG + NADH + H^+	GAP + P_i → BPG	NAD^+ → NADH + H^+
PYR formation	BPG + 2ADP → PYR + 2ATP	BPG → PYR	2ADP → 2ATP
PPYR reduction	PYR + NADH + H^+ → LAC + NAD^+	PYR → LAC	NADH + H^+ → NAD^+
LAC oxidation	LAC + NAD^+ → PYR + NADH + H^+	LAC → PYR	NAD^+ → NADH + H^+
TG lipolysis	TG → 3FA + GLR		
TG synthesis	3FA + GLR + 3ATP → TG + 3ADP + $3P_i$	3FA + GLR → TG	3ATP → 3ADP + $3P_i$
FFA activation	FA + CoA + 2ATP → FAC + 2ADP + $2P_i$	FA + CoA → FAC	2ATP → 2ADP + $2P_i$
PCr breakdown	PCr + ADP + H^+ → Cr + ATP	PCr + H^+ → Cr	ADP → ATP
PCr synthesis	Cr + ATP → PCr + ADP + H^+	Cr → PCr + H^+	ATP → ADP
ATP utilization	H_2O + ATP → ADP + H^+ + P_i		
ADP conversion	ADP ↔ bADP		
Reactions in mitochondria			
β-Oxidation	FAC + 7CoA + $^{35}NAD^+$ → 8ACoA + $^{35}NADH$ + $7H^+$	FAC + 7CoA → 8ACoA + $7H^+$	$^{35}NAD^+$ → $^{35}NADH$
PYR oxidation	PYR + CoA + $^{3}NAD^+$ → ACoA + $^{3}NADH$ + CO_2 + H^+	PYR + CoA → ACoA + CO_2	$^{3}NAD^+$ → $^{3}NADH$ + H^+
CIT formation	ACoA + OAA + H_2O → CIT + CoA + H^+		
α-KG formation	CIT + NAD^+ → α-KG + NADH + CO_2 + H^+	CIT → α-KG + CO_2	NAD^+ → NADH + H^+
SCA formation	α-KG + CoA + NAD^+ → SCA + NADH + CO_2 + H^+	α-KG + CoA → SCA + CO_2	NAD^+ → NADH + H^+
SUC formation	SCA + ADP + P_i → SUC + ATP + CoA	SCA → SUC + CoA	ADP + P_i → ATP
MAL formation	SUC + (2/3)NAD^+ → MAL + (2/3)NADH	SUC → MAL	$^{2}NAD^+$ → $^{2}NADH$
OAA formation	MAL + NAD^+ → OAA + NADH + H^+	MAL → OAA	$^{3}NAD^+$ → $^{3}NADH$ + H^+
Oxidative phosphorylation	$0.5O_2$ + 3ADP + $3P_i$ + NADH + H^+ → H_2O + 3ATP + NAD^+	$0.5O_2$ + H^+ → H_2O	NADH → NAD^+ 3ADP + $3P_i$ → 3ATP

GLU, glucose; G6P, glucose-6-phosphate; GLY, glycogen; GAP, glyceraldyhe-3-phosphate; BPG, 1,3-bisphosphate-glycerate; PYR, pyruvate; LAC, lactate; TG, triglyceride; FA, fatty acid; GLR, glycerol; FFA, free FA; FAC, fatty acyl-CoA; PCr, phosphocreatine; Cr, creatine; CIT, citrate; α-KG, α-ketoglutarate; SCA, succinyl-CoA; SUC, succinate; MAL, malate; OAA, oxaloacetate; ACoA, acety-CoA; bADP, bound ADP.

Table 2. *Species net reaction rates*

Species in Cytosol or Mitochondria Only	
$R_{c,GLU}$	$-\phi_{GLU\rightarrow G6P}$
$R_{c,G6P}$	$\phi_{GLU\rightarrow G6P}+\phi_{GLY\rightarrow G6P}-\phi_{G6P\rightarrow GLY}-\phi_{G6P\rightarrow GAP}$
$R_{c,GLY}$	$\phi_{G6P\rightarrow GLY}-\phi_{GLY\rightarrow G6P}$
$R_{c,GAP}$	$2\times\phi_{G6P\rightarrow GAP}-\phi_{GAP\rightarrow BGP}$
$R_{c,BPG}$	$\phi_{GAP\rightarrow BPG}-\phi_{BPG\rightarrow PYR}$
$R_{c,LAC}$	$\phi_{PYR\rightarrow LAC}-\phi_{LAC\rightarrow PYR}$
$R_{c,TG}$	$\phi_{GLR\rightarrow TG}-\phi_{TG\rightarrow GLR}$
$R_{c,GLR}$	$\phi_{TG\rightarrow GLR}-\phi_{GLR\rightarrow TG}$
$R_{c,FFA}$	$3\times\phi_{TG\rightarrow GLR}-3\times\phi_{GLR\rightarrow TG}-\phi_{FA\rightarrow FAC}$
$R_{c,PCr}$	$-\phi_{PCr\rightarrow Cr}+\phi_{Cr\rightarrow PCr}$
$R_{c,Cr}$	$\phi_{PCr\rightarrow Cr}-\phi_{Cr\rightarrow PCr}$
$R_{m,ACoA}$	$\phi_{PYR\rightarrow ACoA}+8\times\phi_{FAC\rightarrow ACoA}-\phi_{ACoA\rightarrow CIT}$
$R_{m,CIT}$	$\phi_{ACoA\rightarrow CIT}-\phi_{CIT\rightarrow\alpha\text{-}KG}$
$R_{m,\alpha\text{-}KG}$	$\phi_{CIT\rightarrow\alpha\text{-}KG}-\phi_{\alpha\text{-}KG\rightarrow SCA}$
$R_{m,SCA}$	$\phi_{\alpha\text{-}KG\rightarrow SCA}-\phi_{SCA\rightarrow SUC}$
$R_{m,SUC}$	$\phi_{SCA\rightarrow SUC}-\phi_{SUC\rightarrow MAL}$
$R_{c,bADP}$	$\phi_{fADP\rightarrow bADP}-\phi_{bADP\rightarrow fADP}$

Species in Both Cytosol or Mitochondria	Cytosol domain (R_{cj})	Mitochondria domain (R_{mj})
PYR	$\phi_{BPG\rightarrow PYR}+\phi_{LAC\rightarrow PYR}-\phi_{PYR\rightarrow LAC}$	$-\phi_{PYR\rightarrow ACoA}$
FAC	$\phi_{FA\rightarrow FAC}$	$-\phi_{FAC\rightarrow ACoA}$
MAL	$\phi_{c,OAA\rightarrow MAL}$	$\phi_{SUC\rightarrow MAL}-\phi_{m,MAL\rightarrow OAA}$
OAA	$-\phi_{c,OAA\rightarrow MAL}$	$\phi_{m,MAL\rightarrow OAA}-\phi_{ACoA\rightarrow CIT}$
ATP	$-\phi_{GLU\rightarrow G6P}-\phi_{G6P\rightarrow GLY}-\phi_{G6P\rightarrow GAP}+2\times\phi_{BPG\rightarrow PYR}-\phi_{GLR\rightarrow TG}-\phi_{FA\rightarrow FAC}-\phi_{ATP\rightarrow ADP}{}^{ATPase}+\phi_{c,PCr\rightarrow Cr}-\phi_{c,Cr\rightarrow PCr}$	$\phi_{SCA\rightarrow SUC}+6\times\phi_{O_2\rightarrow H_2O}$
ADP	$\phi_{GLU\rightarrow G6P}+\phi_{G6P\rightarrow GLY}+\phi_{G6P\rightarrow GAP}-2\times\phi_{BPG\rightarrow PYR}+\phi_{GLR\rightarrow TG}+\phi_{FA\rightarrow FAC}+\phi_{ATP\rightarrow ADP}{}^{ATPase}-\phi_{c,PCr\rightarrow Cr}+\phi_{c,Cr\rightarrow PCr}-\phi_{fADP\rightarrow bADP}+\phi_{bADP\rightarrow fADP}$	$-\phi_{SCA\rightarrow SUC}-6\times\phi_{O_2\rightarrow H_2O}$
NAD	$-\phi_{GAP\rightarrow BPG}+\phi_{PYR\rightarrow LAC}-\phi_{LAC\rightarrow PYR}+\phi_{c,OAA\rightarrow MAL}$	$2\times\phi_{O_2\rightarrow H_2O}-\frac{35}{3}\times\phi_{FAC\rightarrow ACoA}-\frac{2}{3}\times\phi_{SUC\rightarrow MAL}-\phi_{CIT\rightarrow\alpha\text{-}KG}-\phi_{\alpha\text{-}KG\rightarrow SCA}-\phi_{m,MAL\rightarrow OAA}-\phi_{PYR\rightarrow ACoA}$
NADH	$\phi_{GAP\rightarrow BPG}-\phi_{PYR\rightarrow LAC}+\phi_{LAC\rightarrow PYR}-\phi_{c,OAA\rightarrow MAL}$	$\frac{35}{3}\times\phi_{FAC\rightarrow ACoA}-2\times\phi_{O_2\rightarrow H_2O}+\frac{2}{3}\times\phi_{SUC\rightarrow MAL}+\phi_{CIT\rightarrow\alpha\text{-}KG}+\phi_{\alpha\text{-}KG\rightarrow SCA}+\phi_{m,MAL\rightarrow OAA}+\phi_{PYR\rightarrow ACoA}$
P_i	$2\times\phi_{G6P\rightarrow GLY}-\phi_{GLY\rightarrow G6P}-\phi_{GAP\rightarrow BPG}+\phi_{ATP\rightarrow ADP}+\phi_{FAC\rightarrow FA}$	$-\phi_{SCA\rightarrow SUC}-6\times\phi_{O_2\rightarrow H_2O}$
CoA	$-\phi_{FA\rightarrow FAC}$	$\phi_{ACoA\rightarrow CIT}+\phi_{SCA\rightarrow SUC}-\phi_{PYR\rightarrow ACoA}-7\times\phi_{FAC\rightarrow ACoA}-\phi_{\alpha\text{-}KG\rightarrow SCA}$
O_2	$-\phi_{O_2\rightarrow H_2O}$	
CO_2	$\phi_{PYR\rightarrow ACoA}+\phi_{CIT\rightarrow\alpha\text{-}KG}+\phi_{\alpha\text{-}KG\rightarrow SCA}$	

R, reaction rate; subscripts c and m, cytosol and mitochondria, respectively; ϕ, reaction flux; subscript j; *species;* fADP, free ADP.

tion processes, the controller kinetics go in the opposite direction, for which we define $PS^- = 1/PS^+$ and $RS^- = 1/RS^+$.

Flux balance analysis. Flux balance analysis (FBA) refers to a methodology for calculating intracellular fluxes using a stoichiometric model for the major intracellular reactions and applying mass balances in the steady state on intracellular metabolites (69, 71). FBA consists mainly of three stages. First, a network model of the biochemical pathways to be analyzed is formulated (Fig. 1). The flux values are then estimated either from the literature or from our experiments. Finally, metabolic fluxes not available in the literature are obtained indirectly from experimental data and mathematical relationships derived from reaction stoichiometry and biochemistry. For example, in this model, all of the fluxes affecting pyruvate metabolism were available except pyruvate oxidation; therefore, the flux of pyruvate to acetyl-CoA was calculated from known fluxes using FBA. The flux of fatty acyl-CoA to acetyl-CoA was then determined by assuming that 40% of the production of acetyl-CoA comes from pyruvate oxidation and the rest from fatty acid oxidation. In this way, we can obtain all metabolic flux values included in our model.

MODEL SIMULATIONS

Parameter estimation. Our first objective was to determine parameter values for our model such that numerical solutions of the model equations corresponded to experimental data. Because these data are very sparse relative to the large number of model parameters, standard optimization procedures are not feasible for parameter estimation. The first stage of this parameter estimation process is to use FBA to determine the metabolic fluxes under normal resting conditions. The second stage of the estimation process for the model parameters assumes that the equilibrium parameters in the metabolic fluxes have

values comparable to the steady-state concentrations under normal conditions. These values and the flux values determine the values of the rate coefficients. The third stage of the estimation process requires that model simulations agree with limited experimental data available from human and pig hearts. Parameter values are tuned as needed around their initial estimates to obtain model outputs consistent with known physiological qualitative behavior and in agreement with available experimental data from similar conditions. Consequently, this estimation strategy requires many repeated simulations.

Model simulations of myocardial metabolism should yield outputs that match measured chemical species concentrations and flux changes during the transition from normal to ischemic conditions. The literature and our current research provided a reasonable range of species concentrations under normal, resting steady-state conditions in arterial blood and tissue (Tables 3 and 4). All species concentrations in myocardial tissue and flux values are expressed per gram wet weight of myocardium. In addition, species concentrations in the blood (including interstitial fluid), cytosol, and mitochondria (Table 5) were estimated taking into account the relative volumes (effective volume in the model) of these domains (V_b:V_c:V_m = 13:70:17) (6). The mass balance equations (*Eqs. 3–5*) were divided by the tissue volume, which were incorporated into the rate coefficients (*T* or *V*). We estimated transport fluxes and parameters (Table 6) as well as reaction fluxes and parameters (Table 7) either by using FBA or by simulating various segments of the metabolic pathways and comparing steady-state output values to corresponding experimental data from either the literature or our experiments. We chose *M* and *K* values of the same magnitude of the corresponding concentration values; because flux values are constrained by the physiological conditions imposed by the whole network (56, 72, 75), all parameters were determined within reasonable ranges. For comparison to experimental data, the model parameters on a volume basis were converted to a mass basis assuming the tissue density is 1 g/ml.

Table 3. *Species concentration in tissue*

Species	Concentration	Reference
GLU	1.0	78
G6P	0.171	Estimated
GLY	33.0	17, 37, 44, 63, 65
GAP	0.01	73, 74
BPG	0.04	Estimated
PYR	0.2	7, 40, 50
LAC*	3.88	17, 50
TG	3.12	17
GLR	0.015	Estimated
FFA	0.021	78
FAC	0.014	33
CoA	0.012	30, 66
PCr	8.3	7, 34, 44, 52, 59
Cr	3.5	34
NAD*	0.4	
NADH*	0.045	
ATP*	3.4	17, 18, 34, 44
ADP	0.02	34
bADP	1.51	34
P_i	1.66	11, 34
OAA	0.003	26
MAL	0.168	50, 51, 67
ACoA	0.0012	29, 30
CIT	0.6	41, 67
αKG*	0.03	
SCA	0.0056	30
SUC	0.11	50, 51, 67
O_2	0.963	27, 50
CO_2	20.0	27

Vaues are in μmoles per gram wet weight. *From current research.

Table 4. *Species concentration in arterial blood*

Species	Concentration	Reference
GLU	4.75	2, 3, 12, 25, 44, 46, 55, 78, 80
LAC	0.78	2, 3, 25, 55, 78
FFA	0.62	2, 3, 25, 44, 50, 55, 78
PYR	0.068	3
CO_2	18.0	29
O_2	8.8	48
GLR	0.059	2, 3, 55
TG	0.99	70

Values are in millimolar.

Simulation strategy. After obtaining a consistent set of parameter values under normal, resting steady-state conditions, we simulated responses to ischemia induced by a 60% reduction in coronary blood flow from 1.0 to 0.4 $ml \cdot g^{-1} \cdot min^{-1}$ occurring over 1 min. The mathematical model consists of a system of 46 nonlinear differential equations together with a large number of algebraic flux equations. To simulate the dynamic responses, the equations were solved using DLSODE, a robust implicit integrator for stiff and sparse systems (CASC; http://www.llnl.gov/CASC/odepack/software/dlsode.f). The model system parameters are listed in Table 8. Because the mass balance equations were divided by the tissue volume, the domain volumes were represented as relative volume ($V_j' = V_j/V_{tissue}$, where *j* represents blood, cytosol, or mitochondria and V_{tissue} is the tissue volume). In particular, we simulated the rates of glycogen breakdown and lactate uptake as well as lactate accumulation in the cytosol. These responses provided information necessary for choosing the appropriate cytosolic subdomain volume for glycolysis. Having developed confidence in the model's power to predict responses in agreement with experimental data, we examined the time profiles of the cytosolic and mitochondrial redox states and the dynamics of various fluxes and concentrations that are modulated by these redox states. Specifically, the lactate-to-pyruvate ratio and the rates of fatty acids and pyruvate oxidation were simulated to investigate the correspondence of their time profiles to the dynamics of cytosolic and mitochondrial redox. Finally, we simulated the responses of creatine-to-phosphocreatine and cytosolic and mitochondrial ADP-to-ATP ratios.

Simulation results. To verify that the mathematical model chosen was accurate and reliable from a numerical standpoint, a convergence study of its numerical solution was conducted for a given set of output variables (lactate and glycogen concentrations, net glycogen breakdown, and net lactate output). Because the numerical integrator used in this work (DLSODE) changes step size automatically to maximize efficiency while maintaining prescribed accuracy, the bound of the time step and the error tolerance were changed from 10^{-1} to 10^{-6} and 0.01 to 1 min, respectively. On the basis of the convergence study results, it was concluded that convergence of simulations in the present study is assured because they were

Table 5. *Species concentration in blood, cytosol, and mitochondria*

Species	Blood and Interstitial Fluid Domain		Cytosolic Domain		Mitochondrial Domain	
	Concentration, mM	Mass, %	Concentration, μmol/g wet wt	Mass, %	Concentration, μmol/g wet wt	Mass, %
GLU	4.67	61.3	0.56	38.7		0
G6P		0	0.17	100		0
GLY		0	47.14	100		0
GAP		0	0.014	100		0
BPG		0	0.04	100		0
PYR	0.068	1	0.2	80	0.2	19
LAC	0.62	2.2	5.42	97.8		0
TG	0.99	4.1	4.27	95.9		0
GLR	0.06	15.7	0.015	84.3		0
FFA	0.57	27.9	0.022	72.1		0
FAC		0	0.0084	42 (8, 33)	0.048	58 (8, 33)
CoA		0	0.002	10	0.069	90*
PCr		0	11.8	100	0	0
Cr	0.14	0	5	100	0	0
NAD		0	0.057	10	2.12	90
NADH		0	0.0064	10	0.24	90
ATP		0	4.5	92 (4, 34)	1.61	8 (4, 34)
ADP		0	0.051 (4, 67)	12	1.6 (8, 23)	88
P_i		0	1.89	80	2.0	20
OAA		0	0.001	5	0.017	95*
MAL		0	0.012	5	0.94	95*
ACoA		0	0.0013	23 (8, 33)	0.0016	77 (8, 33)
CIT	0.23	2	2	0.042	3.39	96
aKG		0	0.002	5	0.17	95*
SCA		0		0	0.033	100
SUC		0		0	0.65	100
O_2	7.15	52.6	0.963	38.1	0.963	9.3
CO_2	19.48	12.7	20.0	70.2	20.0	17.1

References are listed in parentheses. *From current research.

performed with an error tolerance of 10^{-15} and a time step bound of 6 s (0.1 min).

The results of the simulations showed that ischemia reduced oxygen uptake (59) and accelerated the rate of glycolysis, which led to a significant decrease in glycogen concentration (from 47 to 8.2 μmol/g) with a time profile in good agreement with experimental data when the relative volume of the glycolytic subdomain ($V_{c,GLY}/V_{cell}$, where V_{cell} is the cell volume) is 0.1 (Fig. 3*A*). Figure 3*A* also shows the effects of this relative volume on the dynamics of glycogen breakdown. For clarity, only simulated values of 0.2, 0.1, and 0.05 are shown. With the increase of relative volume from 0.05 to 0.2, the time for glycogen breakdown to reach steady state increased from 10 to >50 min. However, exclusion of intracellular compartmentation from the model (59) led to very slow dynamics that did not match experimental data from our lab. The best fit of the experimental data for glycogen concentration was with a subdomain pool size of 0.1 (10% of the cellular space) (Fig. 3*A*); this value also gave the best fit for myocardial lactate concentration and uptake. The simulated ischemic response also shows that lactate concentration increased from 5.4 μmol/g at rest to a maximal value of 22.6 μmol/g after 7 min and then decreased gradually to 13.5 μmol/g (Fig. 3*B*). Corresponding experimental data for lactate concentration are too imprecise to judge whether the model with the glycolytic subdomain improves predictability over the model without it. Under the same conditions, simulations with the glycolytic subdomain model showed that with the onset of ischemia there was a rapid switch from lactate uptake to lactate release, with a close fit between simulated results and experimental data (Fig. 3*C*).

Model simulations can also predict distinct transient responses to ischemia of species concentrations in the cytosol and mitochondria for which no in vivo experimental data are available. There are clear distinctions between the cytosol and mitochondria in changes in the redox state ($NADH/NAD^+$) in

Table 6. *Transport rates and model parameter values under normal, resting steady state*

Species	Flux Value	Parameters
GLU	$J^f_{b\to c,\,GLU} = 0.24$	$M_{b\to c,\,GLU} = 4$*, $T_{b\to c,\,GLU} = 0.45$
LAC	$J^f_{b\to c,\,LAC} = 0.66$	$M_{b\to c,\,LAC} = 0.27$*, $T_{b\to c,\,LAC} = 0.95$
	$J^f_{b\to c,\,LAC} = 0.41$	$M_{c\to b,\,LAC} = 150$, $T_{c\to b,\,LAC} = 11.7$
PYR	$J^f_{c\to m,\,PYR} = 0.73$	$M_{c\to m,\,PYR} = 0.2$, $T_{c\to m,\,PYR} = 1.46$
FFA	$J^p_{b\leftrightarrow c,\,FFA} = 0.14$	$\sigma_{b\leftrightarrow c,\,FFA} = 6.74$, $\lambda_{b\leftrightarrow c,\,FFA} = 0.32$
FAC	$J^f_{c\to m,\,FAC} = 0.14$	$M_{c\to m,\,FAC} = 0.79$, $T_{c\to m,\,FAC} = 13.3$
CoA	$J^f_{c\to m,\,CoA} = 0.14$	$M_{c\to m,\,CoA} = 0.79$, $T_{c\to m,\,CoA} = 13.3$
O_2	$J^p_{b\leftrightarrow c,\,O_2} = 5.41$	$\sigma_{b\leftrightarrow c,\,O_2} = 1.0$, $\lambda_{b\leftrightarrow c,\,O_2} = 1.54$
CO_2	$J^p_{b\leftrightarrow c,\,CO_2} = 4.43$	$\sigma_{b\leftrightarrow c,\,CO_2} = 1.0$, $\lambda_{b\leftrightarrow c,\,CO_2} = 8.48$
P_i	$J^f_{c\to m,\,Pi} = 31.5$	$M_{c\to m,\,P_i} = 0.21$, $T_{c\to m,\,P_i} = 35.0$
ATP	$J^f_{m\to c,\,ATP} = 31.5$	$M_{m\to c,\,ATP} = 1.61$, $T_{m\to c,\,ATP} = 63.1$
ADP	$J^f_{c\to m,\,ADP} = 31.5$	$M_{c\to m,\,ADP} = 1.61$, $T_{m\to c,\,ADP} = 63.1$
NADH†	$J^f_{c\to m,\,NADH} = 0.73$	$M_{c\to m,\,NADH} = 0.01$, $T_{c\to m,\,NADH} = 5.01$
NAD†	$J^f_{m\to c,\,NAD} = 0.73$	$M_{m\to c,\,NAD} = 0.01$, $T_{m\to c,\,NAD} = 5.01$

J, transport rate (in $\mu mol \cdot min^{-1} \cdot g\ wet\ wt^{-1}$); *M*, affinity coefficient (in μmol/g wet wt or *mM); *T*, normalized transport rate coeffient (in $\mu mol \cdot min^{-1} \cdot g\ wet\ wt^{-1}$); λ, membrane permeability coefficient (in min^{-1}); σ, partition coefficient. †The transport rates of NADH and NAD equal the transport rate of MAL from cytosol to mitochondria, which is the rate of the MAL-asparate shuttle (not listed).

Table 7. *Reactions fluxes and model parameter values under normal steady state*

Reactions	Flux Values	Parameters			
		$V_{X-Y,Z-W}$	$K_{X-Z,V-W}$	$\mu^{\pm}$	$\nu^{\pm}$
$\phi_{GLU,\,G6P}$	0.24 (78)	1.21	4.0	0.01 (+)	0
$\phi_{G6P,\,GLY}$	0.2 (78)	0.22	0.009	4.41 (+)	0
$\phi_{GLY\text{-}P_i,\,G6P}$	0.2 (78)	3.92	53.29	0.03 (−)	0
$\phi_{G6P,\,GAP}$	0.24	1.45	0.86	0.88 (+)	0
$\phi_{GAP,\,BGP}$	0.48	2.90	0.13	0	0.089 (−)
$\phi_{BPG,\,PRY}$	0.48	2.90	0.2	0.00011 (−)	0
$\phi_{PYR,\,LAC}$	0.26 (58)	3.04	0.06	0	0.9 (+)
$\phi_{LAC,\,PYR}$	0.51 (58)	2.17	8.13	0	6.22 (−)
$\phi_{PYR\text{-}CoA,\,ACoA}$	0.73	1.48	0.00014	0	8.89 (−)
$\phi_{TG,\,GLR}$	0.02 (17, 18)	0.06	1.71	0	0
$\phi_{GLR\text{-}FFA,\,TG}$	0.02 (17, 18)	0.30	0.001	0.88 (+)	0
$\phi_{FA\text{-}CoA,\,FAC}$	0.14	0.16	0.00001	0.88 (+)	0
$\phi_{FAC\text{-}CoA,\,ACoA}$	0.14	2.97	0.066	0	0.089 (−)
$\phi_{ACoA,\,CIT}$	1.85	14.8	0.00019	0	0
$\phi_{CIT,\,\alpha KG}$	1.85	14.8	10.14	0	8.89 (−)
$\phi_{\alpha KG\text{-}CoA,\,SCA}$	1.85	14.8	0.51	0	8.89 (−)
$\phi_{SCA,\,SUC}$	1.85	14.8	0.099	0.011 (−)	0
$\phi_{SUC,\,MAL}$	1.85	14.8	1.74	0	8.89 (−)
$\phi_{MAL,\,OAA}$	1.85	14.8	2.82	0	8.89 (+)
$\phi_{O_{2,\,H_2O}}$	5.41	98.19	13.48	0.0011 (−)	0.011 (+)
$\phi_{ATP,\,ADP}$	31.48	157.36	18	0	0
$\phi_{PCr,\,Cr}$	2.0	88	47.2	0.0013 (−)	0
$\phi_{Cr,\,PCr}$	2.0	88	20	8.82 (+)	0
$\phi_{ADP,\,bADP}$	10	19	0.046	0	0
$\phi_{bADP,\,ADP}$	10	90	12.1	0	0

$V_{X-Y,Z-W}$, maximal reaction rate (μmol·g wet wt^{-1}·min^{-1}); $K_{X-Y,Z-W}$, reaction coefficient (μmol·g wet wt^{-1}·min^{-1})^n, $n = 1, 2$; μ^+, ν^+ associate with C_{ATP}/C_{ADP} or C_{NADH}/C_{NAD}; μ^-, ν^- associate with C_{ADP}/C_{ATP} or C_{NAD}/C_{NADH}. Number in parentheses are References.

response to ischemia. From the dynamics of NADH and NAD^+ concentrations in the cytosol and mitochondria, we can compute the changes of the redox state, $RS^+ = NADH/NAD^+$, in both domains (Fig. 4*A*). Whereas the cytosolic RS_c^+ increases quickly by over an order of magnitude and then falls to a stable level at fivefold above the preischemic control value (Fig. 4*A*), the mitochondrial RS_m^+ increases quickly to about double its resting value (Fig. 4*B*). The dynamic response of the ratio of lactate to pyruvate concentrations in the cytosol (Fig. 4*A*) corresponds closely with the cytosolic RS_c^+ but not to the mitochondrial RS_m^+ (Fig. 4*B*). The mitochondrial RS_m^+ regulates the reaction flux of pyruvate to acetyl-CoA ($\phi_{PYR\text{-}ACoA}$) and effects the reaction flux of fatty acetyl-CoA to acetyl-CoA ($\phi_{FAC\text{-}AcoA}$), both of which decrease markedly as RS_m^+ increases (Fig. 4*B*).

Simulated responses of ADP and ATP concentrations in the cytosol and mitochondria in response to ischemia differ significantly in magnitude. This is evident by changes in the phosphorylation state, $PS^- = ADP/ATP$. The increase of mitochondrial PS_m^- is almost five times that of the cytosolic PS_c^- (Fig. 5). Also, the response of the simulated cystolic creatine state, CS_c = creatine/phosphocreatine, is almost identical to the response of the cytosolic PS_c^-.

Table 8. *System parameters used in model*

Q, ml·g^{-1}·min^{-1}	F	V'_b	V'_c	V'_m
1.0	0.33*	0.13	0.7	0.17

Q, blood flow; F, mixing fraction; V'_b, V'_c, and V'_m, relative volume in blood, cytosol, and mitochondria, respectively. *Estimated.

DISCUSSION

A novel aspect of this mathematical model of chemical species transport and metabolism in cardiac tissue is the distinction of blood-interstitial fluid, cytosolic, and mitochondrial domains as well as a glycolytic subdomain in the cytosol. This multidomain model successfully simulated the activation of glycogen breakdown and the switch to lactate production induced by reduced blood flow in an in vivo experimental system. This finding adds further support to the experimental observation that glycogenolytic and glycolytic enzymes are localized in the vicinity of the sarcolemmal membrane and are not uniformly distributed throughout the cytosol (24, 53, 76, 79). In addition, our simulations show that not distinguishing species values between these domains leads to a relatively poor agreement with the dynamics of glycogen breakdown and lactate production observed experimentally during the transition from normal to ischemic conditions (Fig. 3). A key to this success is the recognition that some chemical species are present at significantly different levels in the cytosol and mitochondria and specifically modulate processes present in the corresponding intracellular compartments. This is evident by analyzing the dynamics of key controllers, $NADH/NAD^+$ and ADP/ATP, under normal and ischemic conditions. Because only some chemical species can be measured and data from biopsies of myocardium and blood samples can be obtained only at relatively few time points during an experiment, model simulations provide a more complete quantitative picture of the underlying metabolic processes.

Model simulations compared with experimental data. Model predictions corresponded closely with our recently published

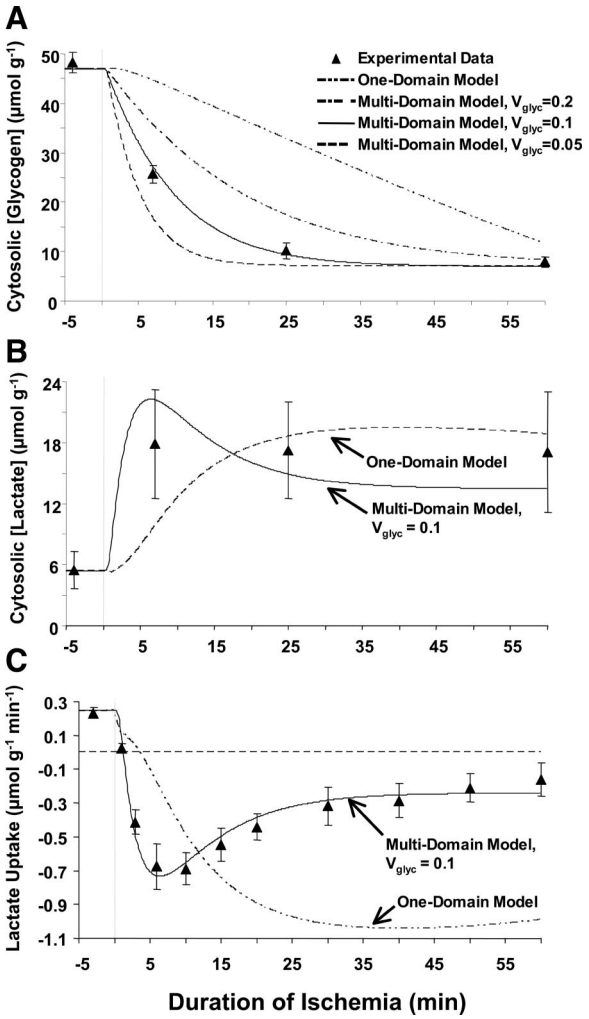

Fig. 3. Metabolic responses to a 60% reduction in coronary blood flow. Data points are from in vivo experimental studies in anesthetized swine (see Ref. 54). The lines represent simulated results (see text for details). *A*: glycogen concentration dynamics. *B*: lactate concentration dynamics. *C*: lactate uptake dynamics. V_{glyc}, glycogen volume.

experimental data (58) on myocardial glycogen content and lactate uptake/release (Fig. 3) when blood flow was reduced by 60% in the left anterior descending coronary artery of anesthetized pigs. The venous effluent was sampled from the anterior interventricular vein, and repeated myocardial biopsies were sampled from the anterior left ventricular free wall. Ischemia reduces the delivery of oxygen to the tissue, which causes mitochondrial metabolic dysfunction by slowing down oxidative phosphorylation and by inhibiting fatty acid and pyruvate oxidation. As a result, mitochondria produce less ATP and anaerobic glycolysis increases using glycogen as its main fuel (65, 68). Two minutes after the onset of ischemia, glycogen breakdown increases rapidly leading to a higher rate of pyruvate production. However, under ischemic conditions, pyruvate produced by anaerobic glycolysis does not readily enter mitochondria and undergo oxidation to acetyl-CoA because this reaction is inhibited by the increase in mitochondrial NADH/NAD^+ secondary to reduced oxygen consumption (68). In the cytosol, the high NADH/NAD^+ drives the conversion of pyruvate to lactate and leads to a rise in the concentration of lactate (Fig. 3*B*), which causes a switch from net lactate uptake to net lactate release (Fig. 3*C*). As glycogen stores are depleted and the rate of glycolysis falls, the NADH-to-NAD^+ ratio also falls, and both tissue lactate concentration and its rate of efflux decrease and reach new steady states (Figs. 3 and 4). These simulated results also agree with experimental studies by other researchers (7, 65).

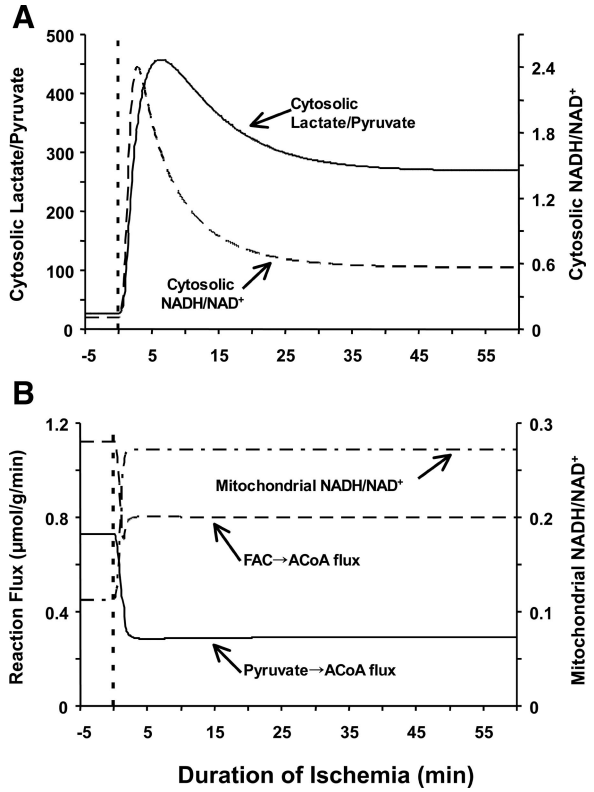

Fig. 4. Computer-simulated values from the multiple-domain model (glycolysis relative volume is 0.1). *A*: cytosolic NADH-to-NAD^+ ratio and the lactate-to-pyruvate ratio. *B*: reaction flux rate of pyruvate to acetyl-CoA (ACoA) and fatty actyl CoA (FAC) to ACoA and the mitochondrial NADH-to-NAD^+ ratio.

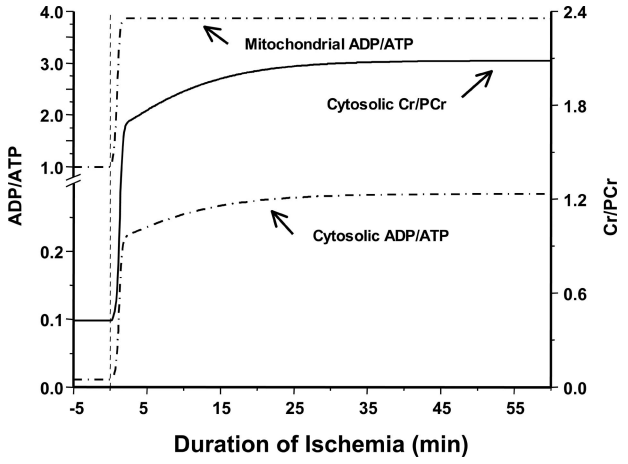

Fig. 5. Model-simulated values of ADP-to-ATP ratios in the mitochondria and cytosol and the cytosolic Cr-to-PCr ratio generated from the multiple-domain model (glycolysis relative volume is 0.1).

Comparison of model simulations from current multidomain and previous one-domain models (59) show a great improvement in predicting the dynamics of glycolysis and lactate uptake during ischemia with our new multidomain model. On the basis of the reaction kinetics used in our model, separation of the cytosol and mitochondria decreases the volume of distribution of most metabolites reducing thereby the time constants of the processes affected, thus accelerating the response of glycolysis to the changes of glycogen concentration and ratio of cytosolic ADP/ATP.

Metabolic channeling of glycolysis. The scientific basis for the improvement in predictive power to simulate dynamic changes in glycogen concentration, as well as in the rates of glycolysis and lactate uptake with moderate ischemia, may be attributed to the presence of multienzyme complexes and the phenomenon of metabolic channeling (4, 24, 32, 45, 49, 53, 76, 77, 79). In an earlier model of cardiac metabolism (59), the cytosol was assumed to be a homogeneous solution in which the glycolytic pathway takes place by random motion of individual enzymes, with free diffusion of reaction intermediates within the intact cell. However, recent studies suggested that this assumption may not be correct. Developments in cell biology have revealed an inhomogeneous cytoplasmic infrastructure at the microscopic level (54, 60), in which enzymes are highly organized (19–22, 43). In particular, it has been demonstrated that glycolytic enzymes can bind together to form a multienzyme complex (8, 19, 42) associated with F-actin (8, 64) or other sites such as microtubules and the cellular membrane (24, 36). The metabolic advantages of these multienzyme complexes include metabolic channeling, which refers to the transfer of products from an enzyme directly to an adjacent active site without entering the bulk solution (4, 32, 45, 49). Metabolic channeling of glycolysis can vastly increase the rate of glycolytic reaction sequences by decreasing the transit times for intermediates between enzymes and by producing local high concentration of intermediates. Model-simulated results showed that with the decrease of effective volume in the mass balance equations representing glycolysis, the rate of glycogen breakdown becomes faster (Fig. 3*A*). The physiological significance of metabolic channeling of glycolysis is that it accelerates the rate of glycogen breakdown induced by ischemia. As a major energy storage in the myocardium, glycogen breakdown rapidly produces a large amount of ATP through anaerobic glycolysis to compensate for the reduced ATP production in the mitochondria and to support cardiomyocyte function (e.g., ion homeostatis and sarcomere shortening).

Control of cardiac metabolism during ischemia. The regulation of myocardial metabolism is affected by many factors including arterial substrates, blood flow, and intracellular processes. Even though fatty acids are the dominant fuel for the heart, optimal cardiac function during ischemia depends on glycolysis and pyruvate oxidation (68). Model simulations show a 28% decrease in fatty acid oxidation with a 60% reduction of blood flow while a much larger (62%) decrease in pyruvate oxidation (Fig. 4*B*). Pyruvate oxidation is catalyzed by pyruvate dehydrogenase (PDH), which is a multienzyme complex located on the inner mitochondrial membrane (57). PDH is inactivated by phosphorylation catalyzed by pyruvate dehydrogenase kinase and is reactivated by hydrolysis of its phosphoserine residue catalyzed by pyruvate dehydrogenase phosphatase (32). Therefore, the rate of pyruvate oxidation in the heart depends on the degree of phosphorylation of PDH as well as the concentrations of substrates.

In large animals, the primary regulator of metabolism through PDH is the ratio of intramitochondrial NADH/NAD^+ rather than inactivation by phosphorylation or the acetyl-CoA-to-free CoA ratio (31, 68). It is important to note that the cytosolic and intramitochondrial concentration changes of NADH and NAD^+ during reduced blood flow in vivo are unknown. Current measurements of these species by tissue biopsies lump the cytosolic and mitochondrial compartments. However, during ischemia, cytosolic and mitochondrial NADH/NAD^+ may display different dynamic behaviors. Indeed, simulations show that with the onset of ischemia, intramitochondrial NADH/NAD^+ increases very rapidly monotonically in an almost step fashion, remaining constant afterward. This is consistent with the fast decrease in the rate or pyruvate oxidation (Fig. 4*B*). In contrast, cytosolic NADH/NAD^+ displays a biphasic behavior; first, it increases several-fold very rapidly and then decreases exponentially to a new level. This dynamic behavior is similar to that of the lactate-to-pyruvate ratio in the cytosol (Fig. 4*A*), which is largely dependent on lactate dehydrogenase and the NADH-to-NAD^+ ratio.

Model limitations and future directions. Although the model distinguished three compartments in myocardial tissue and included most of the key metabolites of intermediary metabolism, it did not link substrate metabolism and ATP hydrolysis with mechanical power generation and heat release. The addition of these parameters would allow for the calculation and comparison of mechanical efficiency under normal and ischemic conditions. Furthermore, to analyze cardiac function during ischemia more precisely, we should separate ischemic from nonischemic tissue to mimic more closely the clinical situation where only a portion of the heart is subjected to ischemia (20~30% of left ventricular mass). Finally, experimental techniques need to be developed to assess metabolite levels in the mitochondrial and cytosolic compartments in vivo so that our simulated results can be validated and hypotheses concerning the regulation of glycolysis, lactate production, and relative rates of pyruvate and fatty acid oxidation can be properly tested. In addition, more powerful constrained optimization methods for large-scale systems are needed to get the best estimates of these parameters.

In conclusion, our multidomain model of myocardial cellular metabolism effectively simulates the dynamic metabolic responses to reduced myocardial blood flow. Model simulations show the importance of distinguishing processes between the cytosol and mitochondria as well as of including a glycolytic subdomain in the cytosol in support of the concept of localization of glycolysis to a subdomain of the cytosol. This model not only simulates the dynamic responses in glycogen depletion and lactate production to ischemia observed in large animal experiments but also predicted changes in mitochondrial and cytosolic NADH/NAD^+ and ADP/ATP. Simulations generated with this model can serve as the basis for new critical experiments to test the validity of mechanisms regulating glycolysis and lactate metabolism during myocardial ischemia.

GRANTS

This research was supported by National Institute of General Medical Sciences Grant GM-66309 to establish the Center for Modeling Integrated Metabolic Systems at Case Western Reserve University.

REFERENCES

1. **Achs MJ and Garfinkel D.** Computer simulation of energy metabolism in anoxic perfused rat heart. *Am J Physiol Regul Integr Comp Physiol* 232: R164–R174, 1977.
2. **Ahlborg G, Felig P, Ahlborg G, and Jorfeld L.** Glucose metabolism during leg exercise in man. *J Clin Invest* 50: 2715–2725, 1971.
3. **Ahlborg G, Felig P, Hagenfeldt L, Hendler R, and Wahren J.** Substrate turnover during prolonged exercise in man: splanchnic and leg metabolism of glucose, free fatty acids, and amino acids. *J Clin Invest* 53: 1080–1090, 1974.
4. **Al-Habori M.** Microcompartmentation, metabolic channelling and carbohydrate metabolism. *Int J Biochem Cell Biol* 27: 123–132, 1995.
6. **Alberts B, Bray D, Lewis J, Raff M, Roberts K, and Watson JD.** *Molecular Biology of the Cell*. New York: Garland, 1994.
7. **Arai AE, Pantley GA, Anselone CG, Bristow J, and Bristow JD.** Active downregulation of myocardial energy requirements during prolonged moderate ischemia in swine. *Circ Res* 69: 1458–1469, 1991.
8. **Arnold H and Pette D.** Binding of glycolytic enzymes to structure proteins of the muscle. *Eur J Biochem* 6: 163–171, 1968.
9. **Arnold MK.** *Physiology of the Heart*. New York: Raven, 1992.
10. **Asimakis GK and Sordahl LA.** Intramitochondrial adenine nucleotides and energy-linked functions of heart mitochondria. *Am J Physiol Heart Circ Physiol* 241: H672–H678, 1981.
11. **Babsky A, Hekmatyar S, Wehrli S, Doliba N, Osbakken M, and Bansal N.** Influence of ischemic preconditioning on intracellular sodium, pH, and cellular energy status in isolated perfused heart. *Exp Biol Med* 227: 520–528, 2002.
12. **Bergman BC, Butterfield GE, Wolfel EE, Lopaschuk GD, Casazza GA, Horning MA, and Brooks GA.** Muscle net glucose uptake and glucose kinetics after endurance training in men. *Am J Physiol Endocrinol Metab* 277: E81–E92, 1999.
13. **Cabrera M, Saidel G, and Kalhan S.** Role of O_2 in regulation of lactate dynamics during hypoxia: mathematical model and analysis. *Ann Biomed Eng* 26: 1–27, 1998.
14. **Cabrera M, Saidel G, and Kalhan S.** Lactate metabolism during exercise: analysis by an integrative systems model. *Am J Physiol Regul Integr Comp Physiol* 277: R1522–R1536, 1999.
15. **Ch'en FF, Vaughan-Jones RD, Clarke K, and Noble D.** Modelling myocardial ischaemia and reperfusion. *Prog Biophys Mol Biol* 69: 515–538, 1998.
16. **Chance B, Garfinkel D, Higgins J, and Hess B.** Metabolic control mechanisms. 5. A solution for the equations representing interaction between glycolysis and respiration in ascites tumor cells. *J Biol Chem* 235: 2426–2439, 1960.
17. **Chandler MP, Huang H, McElfresh TA, and Stanley WC.** Increased nonoxidative glycolysis despite continued fatty acid uptake during demand-induced myocardial ischemia. *Am J Physiol Heart Circ Physiol* 282: H1871–H1888, 2002.
18. **Chavezl PN, Stanley WC, McElfresh TA, Huang H, Sterk JP, and Chandler MP.** Effect of hyperglycemia and fatty acid oxidation inhibition during aerobic conditions and demand-induced ischemia. *Am J Physiol Heart Circ Physiol* 284: H1521–H1527, 2003.
19. **Clarke FM and Master CJ.** The association of glycolytic enzymes with structural proteins of sketletal muscle. *Biochim Biophys Acta* 381: 37–46, 1975.
20. **Clegg JS.** Intracellular water and the cytomatrix: some methods of study and current views. *J Cell Biol* 99: 167s–171s, 1984.
21. **Clegg JS.** Properties and metabolism of the aqueous cytoplasma and its boundaries. *Am J Physiol Regul Integr Comp Physiol* 246: R133–R151, 1984.
22. **Clegg JS.** Metabolic organization and the ultrastructure of animal cells. *Biochim Soc Trans* 19: 986–991, 1991.
23. **Cortassa S, Aon MA, Marban E, Winslow RL, and O'Rourke B.** An integrated model of cardiac mitochondrial energy metabolism and calcium dynamics. *Biophys J* 84: 2734–2755, 2003.
24. **Entman ML, Kanike K, Goldstein MA, Nelson TP, Bornet EP, Futch TW, and Schwartz A.** Association of glycogenolysis with cardiac sarcoplasmic reticulum. *J Biol Chem* 251: 3140–3146, 1976.
25. **Gertz EW, Wisneski JA, Stanley WC, and Neese RA.** Myocardial substrate utilization during exercise in humans. Dual carbon-labeled carbohydrate isotope experiments. *J Clin Invest* 82: 2017–2025, 1988.
26. **Gibala MJ, Tarnopolsky MA, and Graham TE.** Tricarboxylic acid cycle intermediates in human muscle at rest state and during prolonged cycling. *Am J Physiol Endocrinol Metab* 272: E239–E244, 1997.
27. **Guth BD, Wisneski JA, Neese RA, White FC, Heusch G, Mazer CD, and Gertz EW.** Myocardial lactate release during ischemia in swine. Relation to regional blood flow. *Circulation* 81: 1948–1958, 1990.
28. **Guyton AC.** *Textbook of Medical Physiology*. Philadelphia, PA: Saunders, 2000.
29. **Hall JL, Lopaschuk GD, Barr A, Bringas J, Pizzurro RD, and Stanley WC.** Increased cardiac fatty acid uptake with dobutamine infusion in swine is accompanied by a decrease in maloanyl CoA levels. *Circ Res* 32: 879–885, 1996.
30. **Hall JL, Stanley WC, Lopaschuk GD, Wisneski JA, Pizzurro RD, Hamilton CD, and McCormack JG.** Impaired pyruvate osidation but normal glucose uptake in diabetic pig heart during dobutamine-induced work. *Am J Physiol Heart Circ Physiol* 271: H2320–H2329, 1996.
31. **Hansford RG and Cohen L.** Relative importance of pyruvate dehydrogenase interconversion and feed-back inhibition in the effect of fatty acids on pyruvate oxidation by rat heart mitochondria. *Arch Biochem Biophys* 191: 65–81, 1978.
32. **Horton HR, Moran LA, Ochs RS, Rawn JD, and Scrimgeour KG.** *Principles of Biochemistry*. Upper Saddle River, NJ: Prentice Hall, 2002.
33. **Idell-Wenger JA, Grotyohann LW, and Neely JR.** Coenzyme A and carnitine distribution in normal and ischemic hearts. *J Biol Chem* 253: 4310–4318, 1978.
34. **Ingwall JS.** *ATP and the Heart*. Boston, MA: Kluwer Academic Publishers, 2002.
35. **Joshi A and Palsson BO.** Metabolic dynamics in the human red cell. Part II. Interactions with the environment. *J Theor Biol* 141: 529–545, 1989.
36. **Karkhoff-Schweizer RR and Knull HR.** Demonstration of tubulin-glycolytic enzyme interactions using a novel electrophoretic approach. *Biochem Biophys Res Commun* 146: 827–831, 1987.
37. **Kristiansen S, Youn J, and Richter E.** Effect of vanadate on glucose transporter (GLUT4) intrinsic activity in skeletal muscle plasma membrane giant vesicles. *Biochim Biophys Acta* 1282: 71–75, 1996.
38. **LaNoue KF and Schoolwerth AC.** Metabolite transport in mitochondira. *Annu Rev Biochem* 48: 871–922, 1979.
39. **Li Z, Yipintsoi T, and Bassingthwaighte J.** Nonlinear model for capillary-tissue oxygen transport and metabolism. *Ann Biomed Eng* 25: 604–619, 1997.
40. **Mallet RT.** Metabolic protector of cardiac performance. *Proc Soc Exp Biol Med* 223: 136–148, 2000.
41. **Martini WZ, Stanley WC, Huang H, Rosiers CD, Hoppel CL, and Brunengraber H.** Quantitative assessment of anaplerosis from propionate in pig heart in vivo. *Am J Physiol Endocrinol Metab* 284: E351–E356, 2003.
42. **Master CJ.** Interactions between glycolytic enzymes and the cytomatrix. *J Cell Biol* 99: 222s–225s, 1984.
43. **Mastro AM and Hurley DJ.** *In Organization of Cell Metabolism*. New York: Plenum, 1986.
44. **Mcfalls EO, Murad B, Liow JS, Gannon MC, Haspel HC, Lange A, Marx D, Sikora J, and Ward HB.** Glucose uptake and glycogen levels are increased in pig heart after repetitive ischemia. *Am J Physiol Heart Circ Physiol* 282: H205–H211, 2002.
45. **Mendes P, Kell DB, and Welch GR.** Metabolic channelling in organized enzyme systems: experiments and models. *Adv Mol Cell Biol* 11: 1–19, 1995.
46. **Mikines KJ, Richter EA, Dela F, and Galbo H.** Seven days of bed rest decrease insulin action on glucose uptake in leg and whole body. *J Appl Physiol* 70: 1245–1254, 1991.
47. **Morales MF and Smith RE.** On the theory of blood-tissue exchange of inert gases. VI. Validity of approximate uptake expressions. *Bull Math Biophys* 10: 191–200, 1948.
48. **Nielsen HB, Bredmose PP, Stromstad M, Volianitis S, Ouistroff B, and Scher NH.** Bicarbonate attenuates arterial desaturation during maximal exercise in humans. *J Appl Physiol* 93: 724–731, 2002.
49. **Ovadi J.** Physiological significance of metabolic channeling. *J Theor Biol* 152: 1–22, 1991.
50. **Panchal AR, Comte B, Huang H, Kerwin T, Darvish A, Des Rosiers C, Brunengraber H, and Stanley WC.** Partitioning of pyruvate between

oxidation and anaplerosis in swine hearts. *Am J Physiol Heart Circ Physiol* 279: H2390–H2398, 2000.
51. **Panchal AR, Comte B, Huang H, Kerwin T, Darvish A, Des Rosiers C, Brunengraber H, and Stanley WC.** Acute hibernation decreases myocardial pyruvate carboxylation and citrate release. *Am J Physiol Heart Circ Physiol* 281: H1613–H1620, 2001.
52. **Pantley GA, Malone SA, Rhen WS, Anselone CG, Arai A, and Bristow J.** Regeneration of myocardial phosphocreatine in pigs despite continuted moderate ischemia. *Circ Res* 67: 1491–1493, 1990.
53. **Pierce GN and Philipson KD.** Binding of glycolytic enzymes to cardiac sarcolemmal and sarcoplasmic reticular membranes. *J Biol Chem* 260: 6862–6870, 1985.
54. **Porter KR.** The cytomatrix: a short history of its study. *J Cell Biol* 99: 3–12, 1984.
55. **Putman CT, Jones NT, Hultman E, Hollidge-Horvat MG, Bonen A, McConachie DR, and Heigenhauser GJF.** Effects of short-term submaximal training in humans on muscle metabolism in exercise. *Am J Physiol Endocrinol Metab* 275: E132–E139, 1998.
56. **Ramakrishna R, Edwards J, McCulloch A, and Palsson B.** Flux-balance analysis of mitochondrial energy metabolism: consequences of systemic stoichiometric constraints. *Am J Physiol Regul Integr Comp Physiol* 280: R695–R704, 2001.
57. **Randle PJ.** Fuel selection in animals. *Biochim Soc Trans* 14: 799–806, 1986.
58. **Salem JE, Cabrera ME, Chandler MP, McElfresh TA, Huang H, Sterk JP, and Stanley WC.** Step and ramp induction of myocardial ischemia: comparison of in vivo and in silico results. *J Physiol Pharmcol* 55: 519–536, 2004.
59. **Salem JE, Saidel GM, Stanley WC, and Cabrera ME.** Mechanistic model of myocardial energy metabolism under normal and ischemic conditions. *Ann Biomed Eng* 30: 202–216, 2002.
60. **Schliwa M and Van BJ.** Structural interaction of cytoskeletal components. *J Cell Biol* 90: 222–235, 1981.
61. **Sies H.** Nicotinamide nucleotide compartmentation. In: *Metabolic Compartmentation*, edited by Sies H. Toronto, Ontario, Canada: Academic, 1982, p. 205–231.
62. **Soboll S, Cibard A, Keller M, and Hebisch S.** The role of the mitochondrial creatine kinase system for myocardial function during ischemia and reperfusion. *Biochim Biophys Acta* 1100: 27–32, 1992.
63. **Somchit A, Jensen-Waern M, Jacobson M, and Essén-Gustavsson B.** On the carbohydrate metabolic response to an experimental infection with *Brachyspira hyodysenteriae* (swine dysentery). *Scand J Lab Anim Sci* 30: 57–64, 2003.
63a. **Sperelakis N**(Editor). *Cell Physiology Source Book: a Molecular Approach*. San Diego, CA: Academic, 2002.
64. **Srere PA and Ovadi J.** Enzyme-enzyme interactions and their metabolic role. *FEBS Lett* 268: 360–364, 1990.
65. **Stanley WC, Hall JL, Stone CK, and Hacker TA.** Acute myocardial ischemia causes a transmural gradient in glucose extraction but not glucose uptake. *Am J Physiol Heart Circ Physiol* 262: H91–H96, 1992.
66. **Stanley WC, Hernandez LA, Spires D, Bringas J, Wallace S, and McCormack JG.** Pyruvate dehydrogenase activity and malonyl CoA levels in normal and ischemic swine myocardium: effects of dichloroacetate. *J Mol Cell Cardiol* 28: 905–914, 1996.
67. **Stanley WC, Kivilo KM, Panchal AR, Hallowell PH, Bomont C, Kasumov T, and Brunengraber H.** Post-ischemic treatment with dipyruvyl-acetyl-glycerol decreases myocardial infarct size in the pig. *Cardiovasc Drugs Ther* 17: 209–216, 2003.
68. **Stanley WC, Lopaschuk GD, Hall JL, and McCormack JG.** Regulation of myocardial carbohydrate metabolism under normal and ischemic conditions. *Cardiovasc Res* 33: 243–257, 1997.
69. **Stephanopoulos G.** Metabolic fluxes and metabolic engineering. *Metab Eng* 1: 1–11, 1999.
70. **Turcotte LP, Richter EA, and Kiens B.** Increased plasma FFA uptake and oxidation during prolonged exercise in trained vs. untrained humans. *Am J Physiol Endocrinol Metab* 262: E791–E799, 1992.
71. **Varma A, Boesch BW, and Palsson BO.** Stoichiometric interpretation of *Escherichia coli* glucose catabolism under various oxygenation rates. *Appl Environ Microbiol* 59: 2465–2473, 1993.
72. **Vock R, Hoppeler H, Claassen H, Wu DX, Billeter R, Weber JM, Taylor CR, and Weibel ER.** Design of the oxygen and substrate pathways. VI. Structural basis of intracellular substrate supply to mitochondria in muscle cells. *J Exp Biol* 199: 1689–1697, 1996.
73. **Vogt AM, Nef H, Schaper J, Poolman M, Fell DA, Kübler W, and Elsasser A.** Metabolic control analysis of anaerobic glycolysis in human hibernating myocardium replaces traditional concepts of flux control. *FEBS Lett* 517: 245–250, 2002.
74. **Vogt AM, Poolman M, Ackermann C, Yildiz M, Schoels W, Fell DA, and Kübler W.** Regulation of glycolytic flux in ischemic preconditioning: a study employing metabolic control analysis. *J Biol Chem* 277: 24411–24419, 2002.
75. **Weibel ER, Taylor CR, Weber JM, Vock R, Roberts TJ, and Hoppeler H.** Design of the oxygen and substrate pathways. VII. Different structural limits for oxygen and substrate supply to muscle mitochondria. *J Exp Biol* 199: 1699–1709, 1996.
76. **Weiss J and Hilderbrand B.** Functional compartmentation of glycolytic versus oxidative metabolism in isolated rabbit heart. *J Clin Invest* 75: 436–447, 1985.
77. **Weiss JN and Lamp ST.** Cardiac ATP-sensitive K^+ channels. Evidence for preferential regulation by glycolysis. *J Gen Physiol* 94: 911–935, 1989.
78. **Wisneski JA, Gertz EW, Neese RA, Gruenke LD, Morris DL, and Craig JC.** Metabolic fate of extracted glucose in normal human myocardium. *J Clin Invest* 76: 1819–1827, 1985.
79. **Xu KY, Zweier JL, and Becker LC.** Functional coupling between glycolysis and sarcoplasmic reticulum Ca^{2+} transport. *Circ Res* 77: 88–97, 1995.
80. **Zierler K.** Whole body glucose metabolism. *Am J Physiol Endocrinol Metab* 276: E409–E426, 1999.